NASA CONTRACTOR REPORT

NASA CR-1880

ENGINEERING STUDY OF FLEXIBLE BAFFLES FOR SLOSH SUPPRESSION

by Franklin T. Dodge

Prepared by
SOUTHWEST RESEARCH INSTITUTE
San Antonio, Texas 78228
for Langley Research Center

NATIONAL AERONAUTICS AND SPACE ADMINISTRATION • WASHINGTON, D. C. • SEPTEMBER 1971

1. Report No.	2. Government Accession No.	3. Recipient's Catalog No.
NASA CR-1880		

4. Title and Subtitle	5. Report Date
ENGINEERING STUDY OF FLEXIBLE BAFFLES FOR SLOSH SUPPRESSION	September 1971
	6. Performing Organization Code

7. Author(s)	8. Performing Organization Report No.
Franklin T. Dodge	Project 02-2841
	10. Work Unit No.
9. Performing Organization Name and Address	114-08-05-01
Southwest Research Institute San Antonio, Texas	11. Contract or Grant No. NAS1-10074
	13. Type of Report and Period Covered
12. Sponsoring Agency Name and Address	Contractor Report
National Aeronautics and Space Administration Washington, D.C. 20546	14. Sponsoring Agency Code

15. Supplementary Notes

16. Abstract

An engineering analysis and design study was conducted to determine if the potential of flexible baffles for providing high damping per unit weight could be realized under operating conditions in a flight system. The elastic properties of aluminum and a large number of non-metallics were determined at 20°C and -196°C, and those materials having the best combination of elastic properties and reaction insensitivity in liquid oxygen were identified. A design procedure was formulated, with the structural strength of the baffle being estimated by a membrane stress analysis. The weight of a flexible baffle system, including the supporting structure, was shown to be substantially less than that of the equivalent rigid baffle system. Model tests of three flexible baffles were conducted in a 0.76-m (30-in.) diameter tank. Liquid nitrogen was used as the slosh liquid. The tests simulated the 100 reuse cycle of the proposed space shuttle. Results of the test program verified the design procedures.

17. Key Words (Suggested by Author(s))	18. Distribution Statement
Slosh Flexible baffles Cryogenic liquid slosh Flexible, cryogenic slosh baffles	Unclassified - Unlimited

19. Security Classif. (of this report)	20. Security Classif. (of this page)	21. No. of Pages	22. Price*
Unclassified	Unclassified	21	$3.00

*For sale by the National Technical Information Service, Springfield, Virginia 22151

ENGINEERING STUDY OF FLEXIBLE BAFFLES FOR SLOSH SUPPRESSION

By Franklin T. Dodge
Southwest Research Institute

SUMMARY

An engineering analysis and design study was conducted to determine if the potential of flexible baffles for providing high damping per unit weight could be realized under operating conditions in a flight system. The elastic properties of aluminum and a large number of non-metallics were determined at 20°C and −196°C, and those materials having the best combination of elastic properties and reaction insensitivity in liquid oxygen were identified. A design procedure was formulated, with the structural strength of the baffle being estimated by a membrane stress analysis. The weight of a flexible baffle system, including the supporting structure, was shown to be substantially less than that of the equivalent rigid baffle system. Model tests of three flexible baffles were conducted in a 0.76-m (30-in.) diameter tank. Liquid nitrogen was used as the slosh liquid. The tests simulated the 100 reuse cycle of the proposed space shuttle. Results of the test program verified the design procedures.

INTRODUCTION

Guidance and control of a liquid propellant rocket depends to a large extent on the suppression of sloshing. Anti-slosh baffles usually are required to diminish the slosh oscillations by increasing the damping. A typical baffle configuration for current vehicles consists of a stack of stiff annular rings fitted around the inner periphery of the propellant tank. The size of each baffle (ratio of baffle width to tank radius) and the required number of baffles to obtain a desired level of damping are determined from semiempirical relationships, such as the one presented by Miles in reference 1. The minimum required thickness of the baffle is computed by a bending-theory analysis of the stresses induced by the slosh pressures exerted on the baffle; this procedure is summarized in reference 2.

Although these current designs effectively attenuate slosh, the baffles are rather massive and represent a high percentage of the tank weight. It has been suggested, therefore, that the thrust-to-weight efficiency of a rocket could be increased by using lightweight, flexible baffles. In fact, model studies conducted at room temperature indicate that the weight can be reduced by using flexible baffles, and, in many cases, an increase in the damping can be obtained for the same size baffle (references 3, 4, 5, 6, 7, and 8).

The objective of the present investigation is to conduct the detailed engineering analysis, design, and testing of baffle, tank, and cryogenic propellant compatibility required to prove that flexible baffles have the potential to provide high damping per unit weight for operating conditions in a flight system. During the first phase of the study, the elastic properties of a large number of materials were obtained by stress-strain tests run at cryogenic temperatures. The promising candidate materials were then evaluated with regard to the safety of their use in liquid oxygen. A strength analysis based on membrane theory was formulated and used to predict a minimum baffle thickness for specified slosh conditions; a baffle designed in this way has the minimum weight for a given load-carrying capacity, and it also has a large flexibility parameter. During the second phase of the study, three baffles were constructed of different plastic films. Each baffle was installed in a 0.76-m (30-in.) diameter tank and tested in a way that simulated the 100 reuse cycle of the proposed space shuttle. These tests were conducted with liquid nitrogen, which has a density and a boiling temperature similar to liquid oxygen.

SYMBOLS

d_s distance of baffle under free surface, meter

E modulus of elasticity of baffle material, newton/m^2

F	flexibility parameter, defined by eq. (5)
g	acceleration due to gravity or equivalent linear acceleration, m/sec^2
h	liquid depth, meter
K	factor of safety
p_o	average slosh pressure exerted on baffle, newton/m^2
P	period parameter, defined by eq. (4)
r	radius to a given point on deflected baffle, meter
R_m, R_θ	meridional and tangential radii of curvature, meter
R_o	tank radius, meter
s	arc length along deflected baffle, meter
t	baffle thickness, meter
w	baffle width, meter
$\bar{\alpha}$	effective thermal expansion coefficient, m/m-°C
γ	damping factor
ΔT	temperature drop from ambient, °C
$\epsilon_r, \epsilon_\theta$	radial and tangential strains, m/m
ζ_o	slosh wave amplitude, meter
η	flexible baffle efficiency, eq. (6)
θ	circumferential coordinate, radian
μ	Poisson's ratio for baffle material
ρ	density of liquid, kg/m^3
ρ_B	density of baffle material, kg/m^3
σ_r, σ_θ	radial and tangential stresses, newton/m^2
ϕ	slope of deflected baffle at radius r, rad
ω	slosh frequency, rad/sec

PHASE I. ENGINEERING DESIGN AND ANALYSIS

Selection of Flexible Baffle Material

An important aspect of flexible baffle design is the selection of a material that is compatible with the thermal and chemical properties of the cryogenic propellant. The material should retain sufficient flexibility at cryogenic temperatures, and it should not degrade after a long exposure to the propellant nor should it react chemically (burn) with the propellant under any credible operating condition. Because liquid oxygen (LOX) imposes perhaps the most severe combination of low temperature and chemical reactivity, and is the source of the largest slosh loads for the space shuttle, this investigation was concentrated on material selection and baffle design for LOX tanks.

Elastic properties.—Information about the elastic properties of materials at cryogenic temperatures is not abundant; references 9, 10, and 11 present the scattered data available about the common metals and plastics. Consequently, as part of this phase of the study, the elastic properties of soft aluminum and 36 non-metallics, all of which appeared to have desirable elastic properties at room temperature, were determined at both 20°C and −196°C, the boiling temperature of liquid nitrogen. (Liquid nitrogen has a slightly lower boiling temperature than LOX and is slightly less dense but is much safer to handle.) The non-metallics tested were plastic films, fabrics reinforced with fiberglass, and fabrics impregnated with various plastics or rubbers. Two tensile-test specimens of each material were made to the dimensions shown in Figure 1. The thicknesses of the specimens ranged from 5×10^{-5} m (0.002 in.) to about 2.5×10^{-4} m (0.01 in.). Each material was tested in uniaxial tension at a constant strain rate of 0.005 m/m-sec, until fracture occurred. Figure 2 shows the tensile-test apparatus and associated electronics; in the test case shown, the specimen was completely immersed in a bath of liquid nitrogen at −196°C. Typical stress-strain curves obtained from these tests are shown in Figure 3.

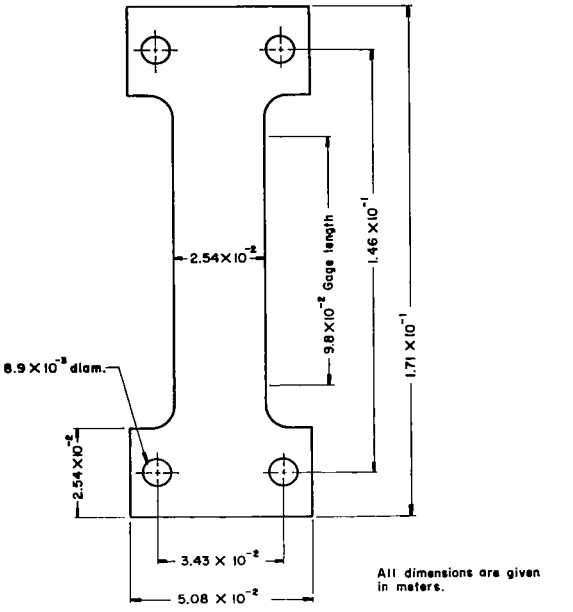

FIGURE 1. DIMENSIONS OF TENSILE TEST SPECIMENS

The plastic films have the most favorable elastic properties of all the materials tested. The density and the coefficient of thermal expansion at 20°C (as tabulated in ref. 9 or in the manufacturer's specifications), the measured yield stress, the ultimate stress, and the elastic modulus for the plastics and the soft aluminum are shown in Table 1. Although the ultimate and yield stresses for most of the plastics are slightly directional and vary somewhat with the thickness of the film, the values given in Table 1 are representative and, furthermore, agree with the few available published data.

To assure that the materials would not fail in fatigue during sloshing, Plastics A and B and aluminum were subjected to a 5000-cycle stress-strain test at −196°C, using the apparatus shown previously in Figure 2. During each cycle, the specimen was strained to a maximum tensile stress of $\sigma_{yield}/2$ and then compressed, with very little stress, to form a "bowed out" circular arc. Owing to the long length of time required to perform the 5000-cycle stress-strain test, the fatigue properties of some of the remaining plastics, namely those that were used in the Phase 2 tests, were evaluated during the actual slosh tests. In no case was a fatigue failure noticed, and it appeared that all the materials could withstand more stress cycles than they would experience in a flight system.

LOX compatibility.—According to data supplied by the manufacturers, Plastic A (a polyester film), Plastic B (a polyimide film), Plastic C (a fluoronated ethylene propylene film), and Plastic E (a polytetrafluoroethylene film) do

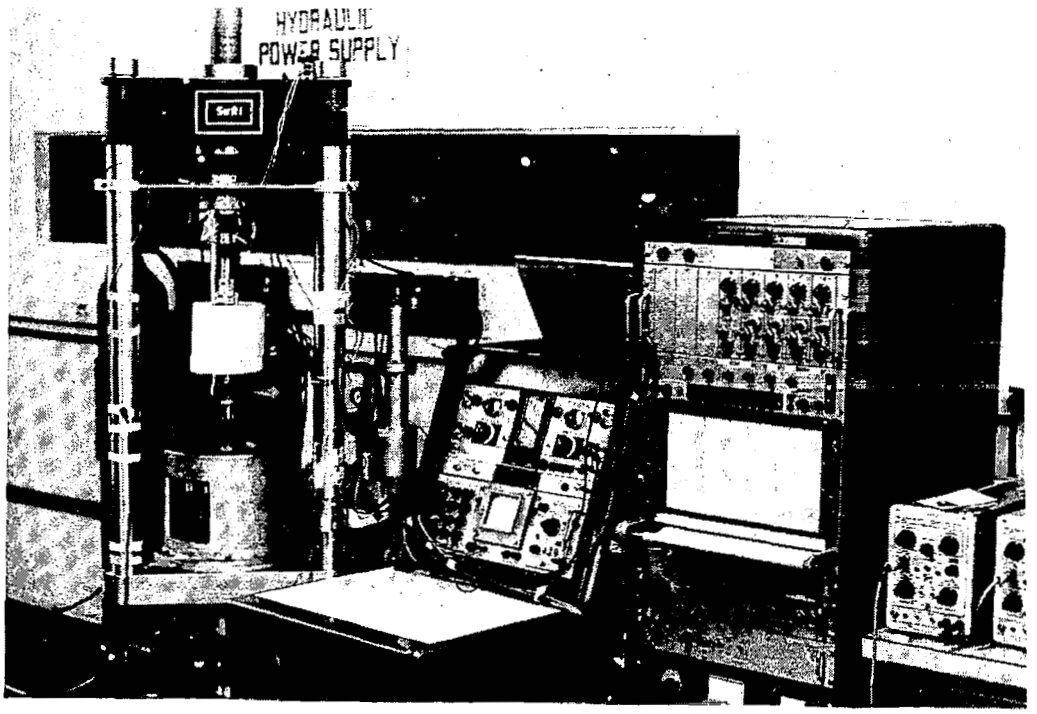

FIGURE 2. VIEW OF TENSILE-TEST APPARATUS

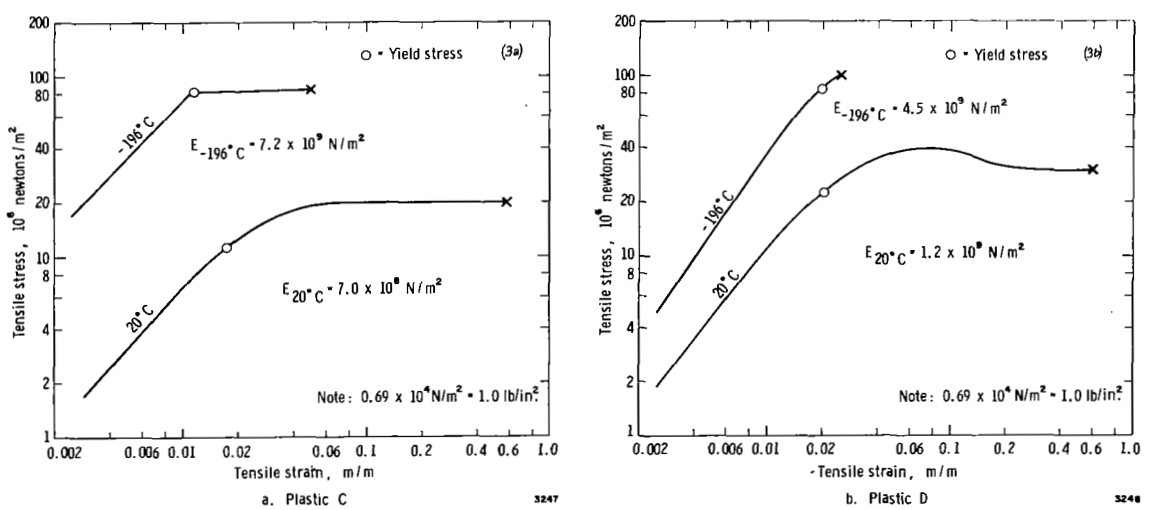

FIGURE 3. TYPICAL STRESS-STRAIN CURVES AT 20°C AND −196°C

TABLE 1. PROPERTIES OF CANDIDATE MATERIALS

			20°C			−196°C			
	ρ_B, kg/m^3	α, m/m − °C	σ_{yield}, newton/m^2	$\sigma_{ultimate}$, newton/m^2	E, newton/m^2	σ_{yield}, newton/m^2	$\sigma_{ultimate}$, newton/m^2	E, newton/m^2	$\rho_B E^{1/2}/(\sigma_{yield})^{3/2}$, kg/newton-m
Plastic A	1.40×10^3	2×10^{-5}	6.2×10^7	13.8×10^7	4.5×10^9	15.2×10^7	17.0×10^7	8.3×10^9	6.8×10^{-5}
Plastic B	1.42×10^3	2×10^{-5}	4.2×10^7	10.4×10^7	3.1×10^9	15.0×10^7	15.0×10^7	5.5×10^9	5.8×10^{-5}
Plastic C	2.15×10^3	8×10^{-5}	1.1×10^7	3.9×10^7	0.7×10^9	8.3×10^7	8.3×10^7	7.2×10^9	24.0×10^{-5}
Plastic D	2.20×10^3	5×10^{-5}	2.1×10^7	3.8×10^7	1.2×10^9	8.5×10^7	10.0×10^7	4.5×10^9	19.0×10^{-5}
Plastic E	2.10×10^3	5×10^{-5}	1.9×10^7	2.1×10^7	1.1×10^9	9.4×10^7	9.9×10^7	4.7×10^9	16.1×10^{-5}
Plastic F	1.65×10^3	20×10^{-5}	2.0×10^7	4.0×10^7	0.5×10^9	19.0×10^7	19.4×10^7	9.8×10^9	6.3×10^{-5}
1100(H14) Alum.	2.70×10^3	2×10^{-5}	14.5×10^7	25.5×10^7	69.0×10^9	16.5×10^7	30.0×10^7	79.0×10^9	43.0×10^{-5}

NOTE: 0.69×10^4 newton/m^2 = 1 lb/in^2.

not degrade after long exposures to LOX. No data were readily available for Plastic D (a polychlorotrifluoroethylene film) or Plastic F (a polyvinylidene chloride film).

Plastic A does not pass the standard LOX reaction test (NASA-MSFC Specification 106, a test in which the material is immersed in LOX and impacted by a striker with an energy of 10 kg-meter, with combustion or the lack of it as the observed quantity), and is not recommended for use with LOX in a man-rated vehicle. For the same reason, the use of Plastic B in its larger thicknesses is questionable although not entirely precluded. In tests at SwRI (ref. 12), Plastic F has been shown to have excellent resistance to combustion in gaseous oxygen, but its ability to pass NASA-MSFC Spec. 106 has not been determined. Of all the tested plastics, Plastics C, D, and E, which are all highly fluoronated, are the most insensitive to impact reaction in LOX.

Relative weight.—The last column in Table 1 lists values of $\rho_B E^{1/2}(\sigma_{yield})^{-3/2}$, a parameter shown later to be proportional to the weight of a flexible baffle made of the material in question. The tabulated values show that a baffle made of any of the plastics will weigh substantially less than an aluminum baffle, although the indicated differences could be reduced by using a high-strength aluminum.

Plastics A, B, and F have the smallest values of $\rho_B E^{1/2}(\sigma_{yield})^{-3/2}$ but, as stated earlier, Plastic A cannot be used safely in LOX, and the large coefficient of thermal expansion for Plastic F, when compared to those of the common tank materials, indicates that thermal stresses would be a problem with it.* Thus, Plastics C, D, and E, with possibly Plastic B as an alternate, have the "best" combination of elastic properties and reaction insensitivity to LOX.

Fabrication.—Plastics C, D, and E are available commercially in rolls or sheets up to about 0.93-m wide (36 in.) and up to about 2.5×10^{-3} m (0.1 in.) thick; Plastic B is available only up to about 1.3×10^{-4} m (0.005 in.) thick. Thus, full-scale baffles probably can be fabricated from these plastics, with the possible exception of Plastic B, without the necessity of making laminations to obtain a thicker sheet; this is a desirable feature since laminating generally increases the LOX impact sensitivity of the material (ref. 13). All four of the plastics can be made into sheets of larger width by joining two or more sheets together with a combination of heat and pressure (heat-sealing). An exhaustive study of fabrication techniques was not attempted during this study, but it was noted during the fabrication of the baffles for the tests in Phase 2 that the heat-sealed bond for Plastic C was as strong as the parent material and the bond for Plastic E, which had an acceptable shear strength, could be "peeled" apart easily.

Strength Analysis

In the Appendix, it is argued that the ability of a flexible baffle to withstand the loads developed during the sloshing is derived primarily from the membrane stresses caused by the deflection of the baffle and that the bending

*Thermal stresses are discussed in the Appendix.

resistance of the baffle is negligible. A stress analysis for a circular-ring baffle, based on membrane theory, is given in the Appendix. The analysis predicts that the maximum stress will not exceed σ_{yield}/K, where $K > 1$ is a factor of safety, if the thickness t of the baffle is at least as large as

$$t_{minimum} = 0.57R_o\left(\frac{w}{R_o}\right)^{1/2}\left(\frac{K^{3/2}E^{1/2}p_o}{\sigma_{yield}^{3/2}}\right) \tag{1}$$

where R_o is the radius of the tank, w is the width of the baffle, and p_o is the average slosh pressure across the width of the baffle. Thermal stresses are neglected in eq. (1), for reasons explained in the appendix. [Eq. (1) proves that, if other things are equal, the weight of the baffle is proportional to $\rho_B E^{1/2}(\sigma_{yield})^{-3/2}$, as was stated earlier.]

The average pressure p_o is related to the width of the baffle, the amplitude ζ_o of the slosh wave, and the depth of submergence d_s of the baffle; in the Appendix, this relation is shown to be

$$p_o = 5.9\rho g R_o\left(\frac{w}{R_o}\right)^{0.485}\left(\frac{\zeta_o}{R_o}\right)^{1.515} e^{-2.79(d_s/R_o)} \tag{2}$$

Slosh Damping

The slosh damping provided by a *rigid* baffle (ref. 1) is

$$\gamma_{rigid} = 2.8\left[\frac{w}{R_o}\left(2-\frac{w}{R_o}\right)\right]^{3/2}\left(\frac{\zeta_o}{R_o}\right)^{1/2} e^{-4.6(d_s/R_o)} \tag{3}$$

where the damping factor γ is the logarithmic decrement divided by 2π. The damping of a rigid baffle, for a given R_o and ζ_o, thus depends only upon w and d_s. For a *flexible* baffle, however, the damping depends not only upon w and d_s but also upon the thickness t, the elastic modulus E, and Poisson's ratio μ (which is about 0.3 for plastic films). The variation of γ with these factors can be conveniently expressed in the graphical form shown in Figure 4 (adapted from ref. 8). It can be seen that, for a given R_o, ζ_o, and w, the flexible baffle damping γ_{flex} is a multiple of the rigid baffle damping γ_{rigid}; the multiple is a function of the "period parameter" P,

$$P = 2\pi\left(\frac{\zeta_o}{w}\right)e^{-1.84(d_s/R_o)} \tag{4}$$

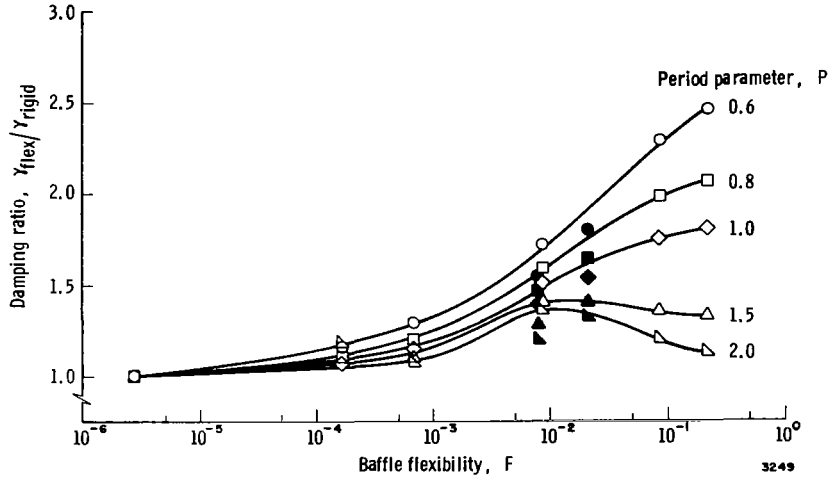

FIGURE 4. RELATIVE DAMPING AS A FUNCTION OF FLEXIBILITY AND PERIOD PARAMETERS (REF. 8)

and the "flexibility parameter" F,

$$F = 0.04\left(\frac{\rho g R_o}{E}\right)\left(\frac{w}{R_o}\right)^5\left(\frac{R_o}{t}\right)^3 \tag{5}$$

The flexibility parameter was originally derived from an elastic-plate bending analysis, but it is apparently a valid way to correlate data even for values of F for which the bending strength of the baffle is negligible.

Design of Flexible Baffle Systems

The minimum damping that must be provided by a baffle system is determined by a stability and control analysis of the rocket, or alternatively by a loads analysis, and by an estimation of the perturbing excitations along the flight path. These analyses give, in addition to the minimum γ, the maximum tolerable value of the slosh amplitude ζ_o. Assuming that the analyses have been performed, so that ζ_o and γ are known, a flexible baffle system can be designed in the following way, in which a realistic set of example conditions is used for the sake of definiteness:

Propellant = LOX, $\rho = 1.14 \times 10^3$ kg/m^3 (71 lb/ft^3)

Baffle material = Plastic C

Tank radius R_o = 2.54 m (100 in.)

Maximum g = $3\,g_o$ = 28.40 m/sec^2 (1120 in./sec^2)

Maximum ζ_o = $0.1\,R_o$ = 0.254 m (10 in.)

Minimum γ = 0.06

These values are representative of the SATURN S-1C design.

Either as a first estimation or as a result of optimizing the spacing of the baffles by the method outlined in reference 15, the baffles are assumed to be spaced uniformly along the tank walls at separation distances of $0.2\,R_o$; this is also typical of the SATURN S-1C. For this separation distance and slosh height, the minimum damping occurs when the baffle nearest the surface is at a depth of $d_s = 0.1\,R_o$. The next closest baffle to the surface is at $d_s = 0.3\,R_o$, and, according to eq. (3), it contributes about 40 percent as much damping as the first baffle. The contributions of all the rest of the baffles are negligible. Thus, if γ for each baffle individually is at least 0.06/1.40 = 0.043, the total slosh damping will be adequate. As a first *guess*, the required width of a flexible baffle that has $\gamma = 0.043$ can be computed from the rigid baffle formula, eq. (3); the width is $0.095\,R_o$ = 0.24 m (9.5 in.). Using this value of w in eq. (2), the slosh pressure is 3.5×10^3 newton/m^2 (0.51 lb/in^2). So, using a factor of safety of 3, eq. (1) shows that the thickness of the Plastic C baffle should be at least $4.5 \times 10^{-4}\,R_o = 1.16 \times 10^{-3}$ m (0.045 in.).

Now that the width and thickness of the baffle have been estimated, the period and flexibility parameters can be computed and the curves given in Figure 4 can be used to make a corrected estimate of the baffle size. In this case, the parameters are $P = 2.0$ and $F = 0.23$. According to Figure 4, then, the flexible baffle has nearly the same damping factor as a rigid baffle of the same width, and, consequently, no corrections to the baffle sizing are needed. In fact corrections to the first estimate will seldom be needed, even for heavily loaded baffles for which F might be as small as 10^{-2}. The reason for this is that P must be at least as large as 2 in order to obtain a significantly large γ (small values of P correspond either to deeply submerged baffles or to small slosh waves), and for such large values of P the effects of flexibility are small. This fact will usually eliminate the need to optimize the baffle with regard to F.

Baffle Efficiency

Weight reduction is the greatest advantage of a flexible baffle. The magnitude of the weight reduction or the efficiency η of the baffle has been defined in reference 8 as the ratio of $(\gamma/t)_{\text{flex}}$ to $(\gamma/t)_{\text{rigid}}$, but, since the rigid and flexible factors are always nearly equal, η is also just the ratio of t_{rigid} to t_{flex}. It is logical to extend this definition to include materials of different densities; thus, the definition of baffle efficiency used here is

$$\eta = \frac{(\rho_B t)_{\text{rigid}}}{(\rho_B t)_{\text{flex}}} \tag{6}$$

and the rigid baffle must have the same width as the flexible baffle.

In order to evaluate η for a given flexible baffle, it is necessary to specify the thickness and the elastic properties that are required to make the baffle "rigid." A definition of rigidity must be rather arbitrary, but one reasonable definition is to require that the baffle be so thick that it acts as an elastic plate rather than as an elastic membrane. As an example, consider a rigid baffle having the same width and damping factor as the Plastic C baffle previously discussed but made of high-strength stainless steel ($\sigma_{\text{yield}} = 6.9 \times 10^8$ newton/m^2, $E = 2.07 \times 10^{11}$ newton/m^2, $\rho_B = 7.85 \times 10^3$ kg/m^3). The elastic plate formulas for a uniformly loaded circular-ring (ref. 16) show that for this baffle the maximum stress will not exceed one-third the yield stress if its thickness is at least $3.32 \times 10^{-3} R_o = 8.4 \times 10^{-3}$ m (0.33 in.). With this definition of rigidity, therefore, the efficiency of the flexible Plastic C baffle is $\eta = 27$; that is, the flexible baffle has only about 4 percent of the weight of the rigid baffle. Another way of defining a rigid baffle is to require that its flexibility parameter be no larger than 10^{-5}, for then the flexibility is sufficiently small that the baffle appears to be rigid (see Fig. 4). Using this definition, the stainless steel baffle must have a minimum thickness of 1.07×10^{-2} m (0.42 in.), and the efficiency of the flexible baffle is 34. Incidentally, a baffle made of Plastic C that is rigid by either of the two definitions has a thickness in excess of 3.8×10^{-2} m (1.5 in.), and the efficiency of the flexible baffle for this case is about 34.

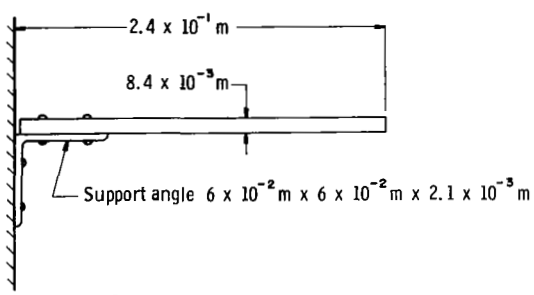

a. Stainless steel rigid baffle

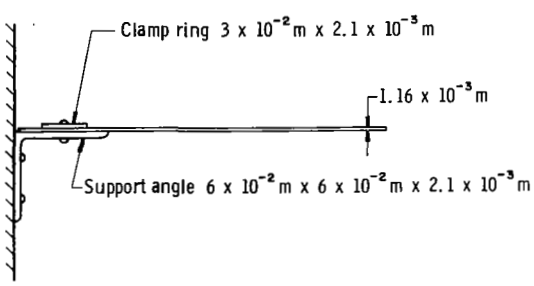

b. Plastic C Flexible baffle

3250

FIGURE 5. SIMPLIFIED BAFFLE SUPPORT SYSTEM

Other ways of obtaining a rigid baffle, such as by decreasing the required thickness and adding stiffeners or longitudinal braces at the inner edge, would probably give similar values of η if the weight of the braces were included in the weight of the rigid baffle.

Only the efficiency of the flexible baffle by itself is represented by eq. (6). A more useful comparison of the weight savings includes the weight of the structure supporting the baffle. Obviously part of the weight savings will be lost if a flexible baffle requires a more massive supporting structure than a rigid baffle. A complete investigation of this problem was beyond the scope of this investigation, but an estimate of the magnitude of the weight savings can be obtained by considering the example of a supporting structure for the previous Plastic C and stainless steel baffles. Figure 5 shows a configuration similar to that used in the model studies reported in reference 8 and in the Phase 2 tests of this study. The support angle, which is assumed to be made of high-strength stainless steel, has been sized approximately to correspond to current design practice and the thickness then selected so that the stresses caused by the slosh load and the baffle weight do not exceed one-third the yield stress. For this arrangement, the efficiency of the Plastic C flexible baffle and its supports is about 8; that is, the flexible baffle and its supports weigh only about 12 percent as much as the rigid baffle and its supports.

Other Considerations

Non-cylindrical tanks.-Propellant tanks used in some space vehicles are not cylindrical, and some of the tanks that are proposed for the space shuttle are not even circular in cross-section. Very little design data for rigid baffles exist for these kinds of tanks (but see Chapter 4, of ref. 17) and almost none exist for flexible baffles. It is perhaps premature in these cases to elaborate a design guide for flexible baffles. Nonetheless, an adequate flexible baffle system for *axisymmetric* tanks could probably be designed by assuming the tank to be a circular cylinder, with its radius equal to the radius of the axisymmetrical tank at the point in question. Tanks that are *almost axisymmetrical* might also be idealized as cylindrical, in this case with a radius such that the cross-sectional area of the cylindrical tank would equal the cross-sectional area of the actual tank.

Tanks with internal insulation.—When the propellant tank is lined internally with thermal insulation, a baffle support system such as the one shown in Figure 5 might result in an excessive number of "heat leaks." Further, other kinds of tanks do not have a sufficient number of "hard points" to mount the baffles in the way shown in Figure 5. In both cases, longitudinal stiffeners or stringers, fixed only to the hard points of the tank, are required to mount the baffle supports. The model tests described in Phase 2 of this study used such a system of longitudinal stringers.

Bubble entrapment.—Flexible baffles offer less possibility of trapping vapor bubbles than do rigid baffles since the buoyancy forces of the bubble tend to cause the baffle to deflect and allow the bubble to vent. The tests conducted during Phase 2 verified this observation.

Tank fueling procedure.—The process of fueling flight tanks can impose severe fluid dynamic loads on baffles. The rigid baffles originally installed in SATURN II-C, for example, were broken out during fueling, and the filling procedure for SATURN 1-C had to be changed to prevent a similar occurrence. Flexible baffles should be less prone to damage during fueling since they will deflect and thereby present less of an obstacle to the flow.

PHASE 2. MODEL TESTS

Verification of the preceding analysis and design procedures by model tests of selected designs was the objective of the Phase 2 investigation.

Model Tank and Instrumentation

The tank used in all the model tests was an aluminum right-circular cylinder, 1.14 m (45 in.) high and 0.76 m (30 in.) in diameter, with a wall thickness of 3.2×10^{-3} m (0.125 in.). As shown in Figure 6, aluminum plates, 1.60×10^{-2} m (0.625 in.) thick, were bolted to flanges on the cylindrical section to form the top and bottom of the tank; the figure also illustrates the ice formation created during a typical test. A viewing port, 0.20 m (8 in.) long by 2.2×10^{-2} m (0.875 in.) wide, was located at a distance of 0.76 m (30 in.) above the bottom of the tank. The viewing port, a double layer of plexiglass, was kept free of ice during the tests by evacuating the space between the two layers with a vacuum pump and spraying the outer layer with "windshield deicer." The tank was filled through the bottom plate by a flexible piping system connected to a large reservoir of liquid nitrogen. A vent pipe in the upper plate was used to prevent the tank pressure from rising above 6.9×10^4 newton/m^2 (10 lb/in^2).

Four support legs were used to mount the tank on a mechanical shake table. Strain gages on one of the support legs formed a load cell to sense the overturning moment exerted on the tank by the sloshing liquid.

The slosh amplitude during a test was estimated by two methods. The inside wall of the tank was marked at intervals of 2.54×10^{-2} m (1.0 in.), so visual observations through the viewing port gave one determination of the amplitude. Also, liquid oxygen condensed on the part of the outside tank wall corresponding to the part of the inside wall wetted by the slosh wave. Thus, by carefully scraping off the outer ice formation, the maximum upward trace of

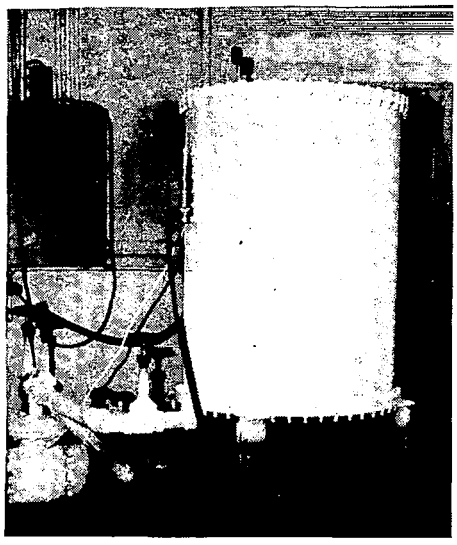

FIGURE 6. VIEW OF 0.76 m DIAMETER SLOSH TANK

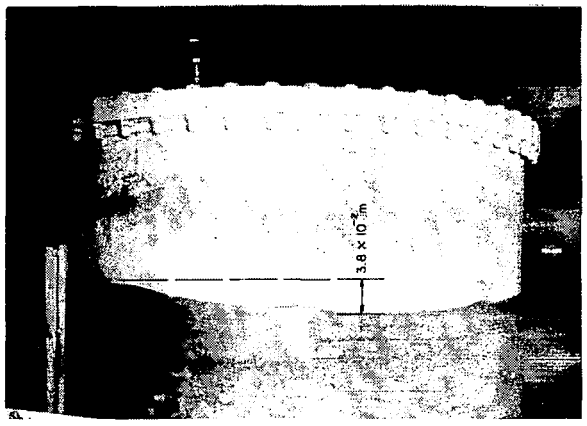

FIGURE 7. SLOSH WAVE TRACE ON TANK WALL

the wave could be seen directly on the tank wall, as is illustrated in Figure 7; in the case shown in the figure, the zero-to-peak amplitude was measured to be 3.8×10^{-2} m (1.5 in.).

Baffle Support Structure

In order to make the design realistic, the model tank was assumed to have hard points only at the top and bottom. Eight box-section stringers, spaced equally around the circumference, were attached to the hard points, and the angle supporting the baffle was attached only to the stringers and not to the tank itself. Figure 8 shows a photograph of this structure, with a baffle in place. The baffle support angle was located 0.76 m (30 in.) above the bottom of the tank, so that the baffle would be centered in the viewing port. Other pertinent dimensions are given in Figure 9.

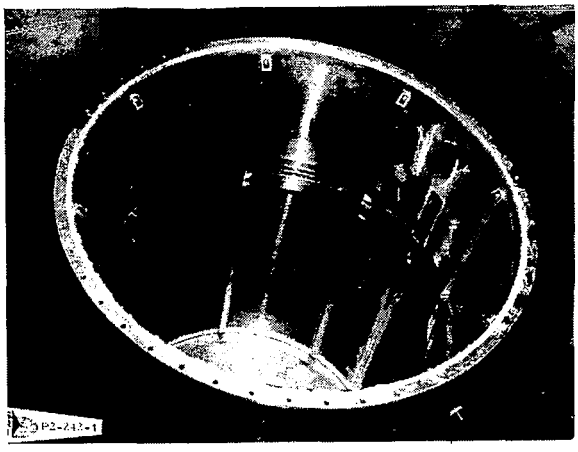

FIGURE 8. INTERIOR VIEW OF TANK AND BAFFLE SUPPORTS

The structure originally was sized in accordance with the expected slosh loads. However, the loads for a tank of this diameter are so small that the stringers and the support angle could not be obtained in the design thicknesses; thus, the smallest available sizes were used instead. The result of these substitutions is that the structure is overdesigned, and therefore overweight, by at least a factor of five.

Design of Model Baffles

Model baffles were fabricated from Plastics B, C, and E, three of the four plastic films

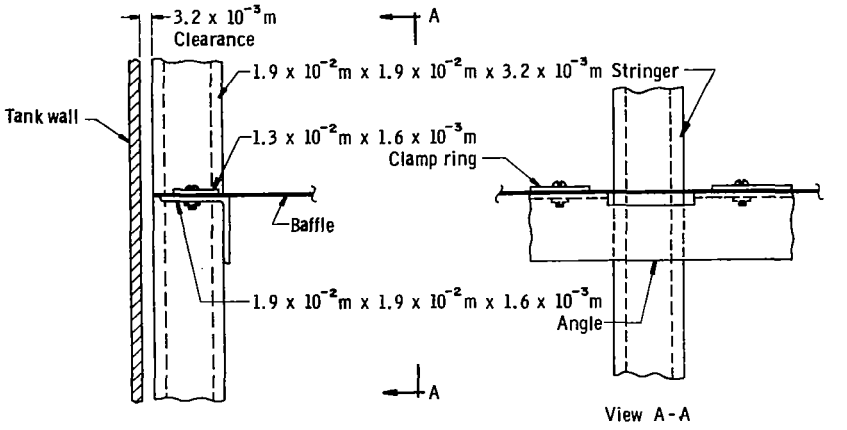

FIGURE 9. BAFFLE SUPPORT STRUCTURE

recommended in Phase 1. The other recommended plastic, Plastic D, has chemical and elastic properties so similar to Plastic E that it did not seem to be worthwhile to test it separately.

The design slosh conditions originally were picked to be $\zeta_o = 0.1\,R_o$ (3.8×10^{-2} m), $d_s = 0.1\,R_o$ (3.8×10^{-2} m), and $\gamma = 0.06$, which seem to be representative of the SATURN S-1C design. From eq. (3), the required baffle width for these conditions is $w = 0.12\,R_o$ (4.56×10^{-2} m). Since the baffle support angle is itself 1.9×10^{-2} m wide (Fig. 9), a baffle with a width of only 4.56×10^{-2} m would probably be too stiff to be realistic, and the width was therefore increased to 5.80×10^{-2} m ($\approx 0.15\,R_o$). This increased the design damping factor to $\gamma = 0.084$.

The slosh pressure was computed by eq. (2) to be about 1.68×10^2 newton/m^2 (0.024 lb/in^2). With this load and a factor of safety of 3, the minimum thickness of the baffles [eq. (1)] should be 2.9×10^{-6} m (1.2×10^{-4} in.) for Plastic B, 8.3×10^{-6} m (3.3×10^{-4} in.) for Plastic C, and 5.5×10^{-6} m (2.2×10^{-4} in.) for Plastic E. Although the materials are made in a thickness as small as 1.27×10^{-5} m (5×10^{-4} in.) which, however, is still somewhat thicker than required, they could not be obtained in any of the smaller thicknesses during the time allotted for this investigation. Once again, substitutions had to be made; the actual thicknesses were 7.62×10^{-5} m (3×10^{-3} in.) for Plastic B, 5.08×10^{-5} m (2×10^{-3} in.) for Plastic C, and 12.7×10^{-5} m (5×10^{-3} in.) for Plastic E. The unfortunate consequence of the substitutions was that the apparent factor of safety at the design slosh condition of $\zeta_o = 0.1\,R_o$ and $d_s = 0.1\,R_o$ was more nearly 10 than 3. During the tests, this overdesign of the baffles was at least partially compensated for by subjecting the baffles to the more severe off-design conditions of $\zeta_o \approx 0.2\,R_o$ at $d_s = 0.2\,R_o$; the apparent factor of safety for these tests was only about 5. Also, the baffles were subjected to a large number of cycles of wave impact when the liquid level was at the baffle location, which imposes a relatively severe load on the baffle.

Plastics C and E could not be readily obtained in sheets wider than 0.46 m (18 in.). Thus, these two baffles had to be fabricated in halves and joined together as shown in Figure 10; the other pertinent dimensions of the baffles are also shown on this figure. The heat-sealed joint for both Plastic C and Plastic E appeared to be as strong for in-plane tensile forces as the plastic itself, but the Plastic E joint could be peeled apart by transverse forces. The overlapped area (see Figure 10) was always located in the tank at the nodal point of the slosh wave, although this was not really necessary since the support angle and clamp ring provided more than enough restraint to the two halves even without heat-sealing the joint. All three baffles were cut out with a sharp razor blade from a common template. No attempt was made to smooth out rough edges or nicks that might have been created during the fabrication.

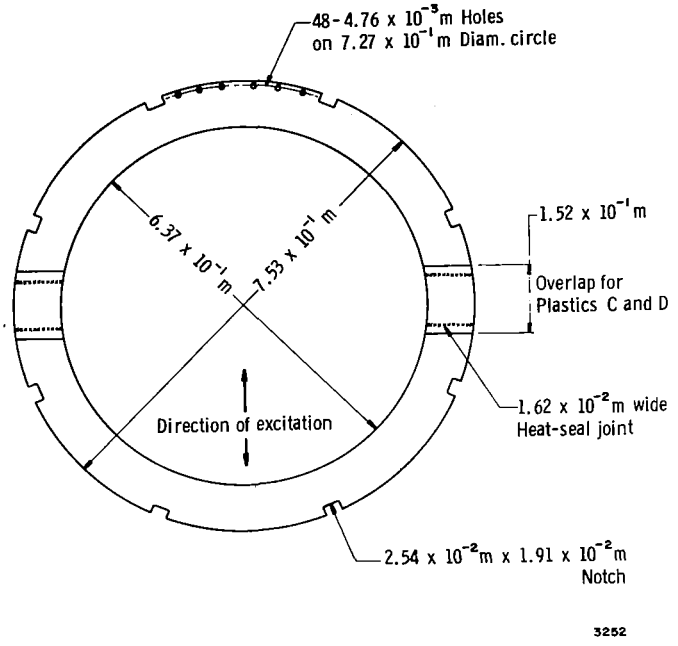

FIGURE 10. DIMENSIONS OF MODEL BAFFLES

TABLE 2. PARAMETERS OF MODEL BAFFLES

Material	w'/R_o	R_o/t	F	Design Conditions		
				P at $\zeta = 0.1\,R_o$	$\gamma_{flex}/\gamma_{rigid}$ (Fig. 4)	γ_{rigid}
Plastic C	0.108	7150	0.120	3.5	≈ 1.15	0.084
Plastic B	0.108	4750	0.035	3.5	≈ 1.30	0.084
Plastic E	0.108	2850	0.009	3.5	≈ 1.20	0.084

Other relevant information about the baffles is presented in Table 2. The flexibility parameters were computed using only the width w' of the baffle that extended beyond the support angle, as is suggested in reference 8. The flexibility parameters are smaller than was desired because the thicknesses are too large; this accounts for the fact that $\gamma_{flex}/\gamma_{rigid}$ is substantially greater than one for all the baffles.

Test Procedure

At the start of each test, it was necessary to chill the entire apparatus with liquid nitrogen from the reservoir for at least 45 minutes in order to prevent immediate vaporization of the entering liquid nitrogen. As soon as liquid began to collect in the tank, however, the filling proceeded rapidly. (In fact, the rate of flow was great enough to form a liquid jet that subsequently impacted the baffle when the liquid level was just approaching the baffle; this in itself was a severe test of the baffle's structural integrity.) The tank was filled to a level d_s above the baffle of about $0.3\,R_o$ to allow for losses due to boiling. As the liquid boiled off, slosh tests were conducted at several liquid levels, until the liquid was below the baffle. The rate of boil-off was about 1.2×10^{-2} m (0.5 in.) per minute, a rate so slow that the boiling did not interfere with the sloshing in any way.

To determine the damping, the shake table was actuated at the slosh natural frequency of about 1.05 cycles/sec, and a constant sinusoidal excitation was maintained until steady-state sloshing was obtained. It was found that a shake table displacement of 1.27×10^{-2} m (0.5 in.) zero-to-peak would produce a slosh wave with about the desired amplitude of $\zeta_o = 0.1\,R_o$ (3.8×10^{-2} m) for $d_s = 0.1\,R_o$. This shake table displacement was then used in all the tests. After obtaining steady-state sloshing, the tank was quick-stopped, using a shear-pin fixture in the

driver arm of the shaker, and the free decay of the liquid motion was recorded with the load cell. The procedure was repeated several times at each liquid level to get an average value of the damping.

The original planning of the program included tests in which each baffle would be subjected to 100 cycles of filling the tank, sloshing, and draining the tank, each time allowing the entire apparatus to come to room temperature, thus simulating the thermal shocks that would be encountered in the 100 reuse cycle of the space shuttle. But the time required for each cycle was over 2 hours, so the tests were abandoned after only ten cycles of testing with the first baffle (Plastic B). There was no evidence of any thermal shock damage at the end of the ten cycles. During the remaining tests, the tank was refilled only as necessary to make up for boil-off losses. However, each baffle was subjected to over 2500 slosh cycles of varying ζ_o and d_s; these tests were more than adequate to simulate the total slosh loads that any individual baffle should experience during the 100 cycle reuse life of the space shuttle.

Results

There was no evidence that any of the baffles suffered structural damage or tearing at the edges from any of the slosh loads, thermal stresses, thermal shocks, or wave impacts. Since the thermal stresses are independent of the baffle thickness, these tests were a realistic simulation of this part of the baffle environment even though the baffles were too thick. The maximum stresses due to the slosh loads were unavoidably too small by about a factor of at least 1.5, since the baffles had to be constructed in larger than the desired thicknesses, but the simulation was close enough to give confidence in the design procedure.

The measured values of slosh damping agreed fairly well with predicted values. Figure 11 shows a typical record of the slosh decay and indicates the way in which the damping factors were computed from the

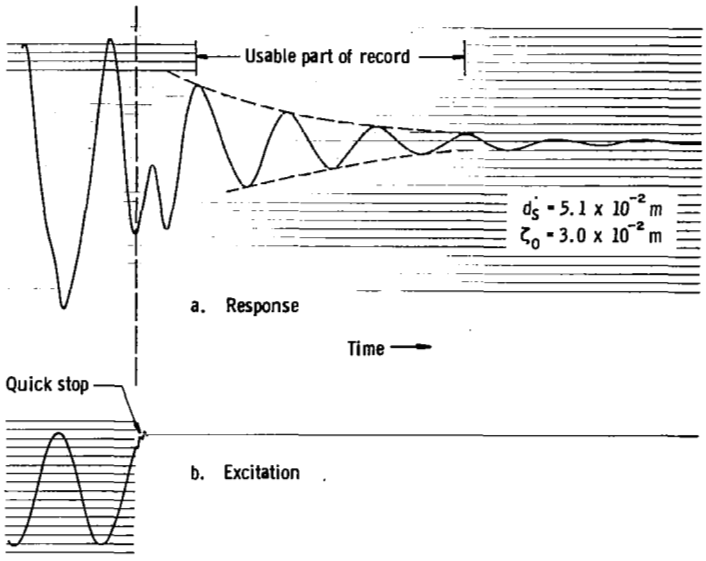

FIGURE 11. TYPICAL SLOSH-DECAY RECORD, PLASTIC B

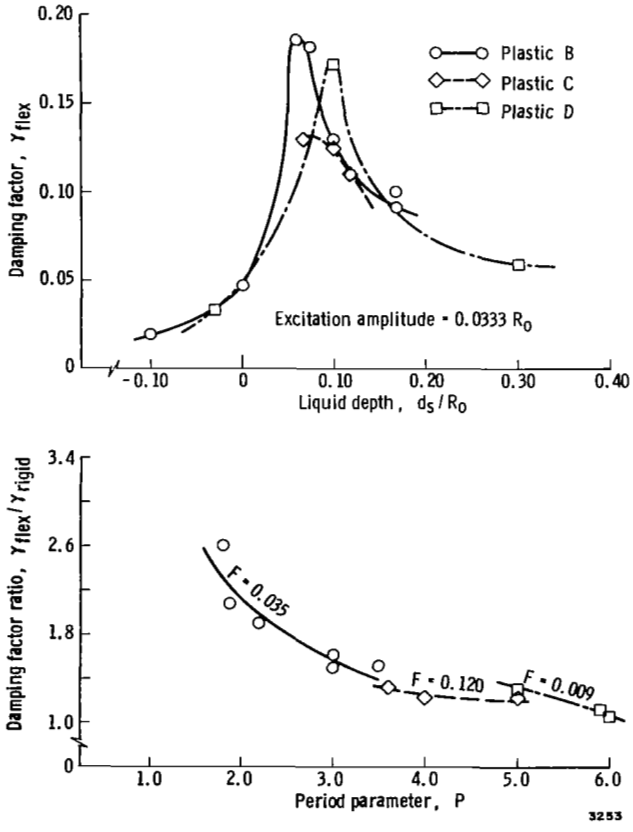

FIGURE 12. DAMPING FACTORS FOR FLEXIBLE BAFFLES

logarithmic decrements. Damping factors for the three baffles tested are shown in the upper half of Figure 12, as a function of liquid depth above the baffle. The damping generally increases as the liquid depth decreases, but when $d_s/R_o \lesssim 0.1$ the slosh wave is not in contact with the baffle over the entire slosh cycle and the damping decreases markedly; this also holds true for rigid baffles (ref. 17). The influence of the period and flexibility parameters on the relative damping is shown in the re-plot of the data on the lower half of Figure 12. The curves, which agree roughly with the more extensive curves given previously in Figure 4, demonstrate again that for $P \gtrsim 3.0$, the relative damping $\gamma_{flex}/\gamma_{rigid}$ is nearly equal to one. (In every case, the viscous damping due to the washing of the liquid on the tank walls did not amount to more than about $\gamma = 0.0004$, which is a negligibly small contribution to the total.

CONCLUSIONS

An engineering analysis and design study was conducted to determine if the potential of flexible baffles for providing high damping per unit weight could be realized under operating conditions in a flight system. The following specific conclusions are offered as a result of this study:

(1) At least three lightweight plastic films (fluoronated ethylene propylene, polytetrafluoroethylene, and polychlorotrifluoroethylene) and possibly a fourth (polyimide) have the combination of good elastic properties at cryogenic temperatures and reaction insensitivity in liquid oxygen that is required to make it possible to design a flexible baffle.

(2) An optimum flexible baffle designed by the membrane analysis developed herein has a large flexibility parameter of about 0.1 or 0.2.

(3) A flexible baffle designed by the method outlined herein will have a damping factor at least as great as that of a rigid baffle of the same width and will weigh considerably less; in the example cited, the flexible baffle had a weight equal to only 4 percent of the rigid baffle weight.

(4) Substantial weight savings are realized even if the weights of the supporting structure of the flexible of the rigid baffle are included in the calculations; the flexible baffle system cited as an example had a weight of only about 12 percent of the rigid baffle system.

(5) Model tests of three different flexible baffles in a 0.76-m (30. in.) diameter tank, with liquid nitrogen as the simulated propellant, indicate that thermal stresses (due to the mismatch in the thermal expansion coefficients of the plastic films and the aluminum tank) should not be large enough to cause thermal shock problems in a flight system.

(6) No structural or fatigue damage to the flexible baffles was observed during a simulated 100 reuse cycle of the proposed space shuttle.

(7) Calculations of the damping provided by the flexible baffles show that previous empirical correlations (ref. 8) of the damping as a function of period parameter and flexibility parameter can be extended to cryogenic temperatures.

ACKNOWLEDGEMENT

Several staff members at SwRI contributed greatly to parts of this program. Mr. Tom Dunham organized the material properties tests for the plastic films. Mr. P. A. Cox conducted the part of the stress analysis concerned with the finite-element computer program. Mr. Luis R. Garza and Mr. Guido E. Ransleben, Jr., designed the experimental apparatus for the Phase 2 model tests.

Southwest Research Institute
Department of Mechanical Sciences
8500 Culebra Road, San Antonio, Texas, March 31, 1971.

APPENDIX A

STRESS ANALYSIS OF A CIRCULAR-RING FLEXIBLE BAFFLE

Basic equations.—The stresses in the flexible baffle are analyzed under the assumptions that membrane theory is applicable and inertia effects due to the baffle motion are negligible. The membrane approximation is justified by the negligible bending rigidity of a thin, flexible baffle, and the internal material damping of a plastic baffle is sufficiently large and the slosh frequency is usually sufficiently high in comparison to the baffle natural frequency that the assumption of negligible inertia effects is valid.

The maximum stresses in the baffle occur at the locations where the average slosh pressure on the baffle is the greatest—under the antinodes of the slosh wave. These maximum stresses can be calculated very closely on the basis of an axisymmetric theory, since the slope of the deflected baffle in the circumferential direction is only about $w/\pi R_o < 0.05$ as large as the slope in the radial direction directly under the antinode.

Figure 1-A shows an element of the baffle in the deflected position. In this sketch, the arclength s is measured along the baffle width and the angle ϕ represents the slope of the element. A force balance in the plane of the element shows that, as $\Delta r \to 0$, $\Delta s \to 0$, and $\Delta\theta \to 0$, the stresses must satisfy the equilibrium relation:

$$\frac{d\sigma_r}{ds} + \frac{(\sigma_r - \sigma_\theta)\cos\phi}{r} = 0 \tag{1-A}$$

The force balance in the direction normal to the element, which must account for the curvature of the element, has been shown by Den Hartog (ref. 18) to be

$$\frac{\sigma_r}{R_m} + \frac{\sigma_\theta}{R_\theta} = \frac{p}{t} \tag{2-A}$$

where $R_m = ds/d\phi$ is the meridional radius of curvature and $R_\theta = r/\sin\phi$ is the tangential radius of curvature.

The boundary condition on the stresses is that $\sigma_r = 0$ at the inner edge of the baffle.

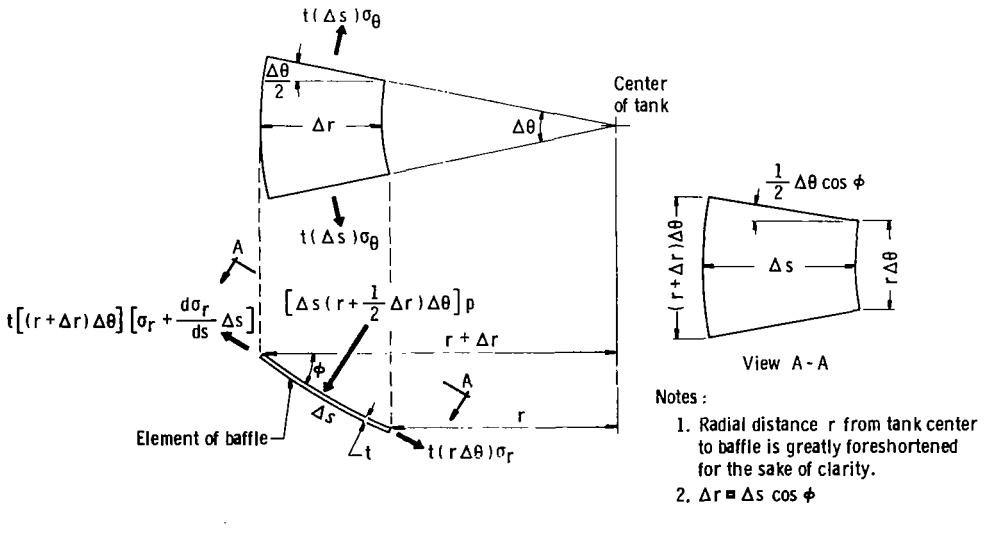

FIGURE 1-A. ELEMENT OF DEFLECTED BAFFLE

The strains induced in the deflected baffle must satisfy Hooke's law:

$$\epsilon_r = \frac{1}{E}(\sigma_r - \mu\sigma_\theta)$$
$$\epsilon_\theta = \frac{1}{E}(\sigma_\theta - \mu\sigma_r) \qquad (3\text{-A})$$

Since the strains can be computed independently from geometric considerations (as will be shown), eqs. (3-A) give two further relations between the σ_r and σ_θ stresses.

The pressure p acting on a circular-ring flexible baffle cannot be calculated exactly from any measurements or analytical methods known to the writer. (The measurements of the pressures on a rectangularly shaped flexible baffle by Schwind, et al., ref. 5, apparently are the only pressures ever measured on a flexible baffle). Consequently, it is assumed here that p can be predicted with adequate conservatism by the results for a rigid baffle given in ref. 14. The average pressure across the width of a rigid baffle is $p_o = C\rho\omega^2\zeta^2$, where C is a nondimensional parameter that depends only on the period parameter, $P = 2\pi\zeta/w$; the best fit of the data for $1 \leqslant P \leqslant 20$ is $C = 7.8\,P^{-0.485}$. In this equation, the slosh frequency ω is $[1.84(g/R_o)]^{1/2}$ and the amplitude of the motion ζ at the baffle location is $\zeta_o e^{-1.84(d_s/R_o)}$, where d_s is the submergence depth of the baffle, and ζ_o is the slosh wave amplitude. (In all the equations, the liquid level in the tank is assumed to be so large that bottom effects are negligible.) Thus, the pressure is

$$p_o = 5.9\,\rho g R_o \left(\frac{w}{R_o}\right)^{0.485} \left(\frac{\zeta_o}{R_o}\right)^{1.515} e^{-2.79\,(d_s/R_o)} \qquad (4\text{-A})$$

Equation (4-A) gives the average pressure; the actual pressure distribution is nearly parabolic across the baffle width.

Approximate solution.—The solution of eqs. (1-A), (2-A), and (3-A) cannot be obtained in closed form, even if the pressure is assumed to be constant across the baffle width. A finite-element computer program was used to solve the equations numerically, but later it was discovered that an approximate solution could be obtained by assuming that (1) the baffle deflects into an arc of a circle, which physically just means that a certain kind of pressure distribution, not necessarily parabolic, is imposed on the baffle, and (2) higher powers of the ratio w/R_o can be neglected in the

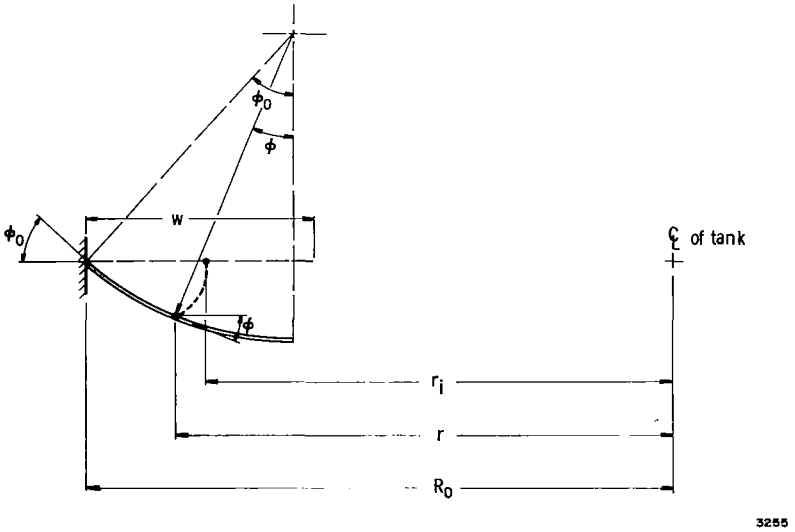

FIGURE 2-A. NOMENCLATURE FOR THE APPROXIMATE STRESS ANALYSIS

equations. The approximate solution gives results that are almost identical to the finite-element program and is much more convenient to use. Thus, it is outlined below.

Figure 2-A shows the deflected baffle. The deflected shape must have a horizontal tangent at the inner edge in order to cause the pressure loading to be zero at this point, a requirement which helps the assumed pressure distribution to approximate more closely the true parabolic pressure distribution. That a horizontal tangent at the inner edge causes the pressure to be zero at this point can be seen from eq. (2-A) if it is realized that $\sigma_r = 0$ and $R_\theta = r/\sin\phi = r/\sin 0° = \infty$ at the inner edge.

The relation between σ_r and σ_θ can be obtained by evaluating ϵ_θ from the geometry of the deflected baffle. Assuming that the strains are small, the ϵ_θ strain is $(r - r_i)/r_i$. Also, the radius to the point where the strain is evaluated is $r = R_o - R_m(\sin\phi_o - \sin\phi)$. The meridional radius of curvature, R_m, is a constant and equal to w/ϕ_o, where ϕ_o is the angle the deflected baffle makes with the normal to the tank wall, at the outer edge of the baffle. The initial radius r_i to the same point can be written in terms of deflected baffle parameters and the radial strain:

$$r_i = R_o - R_m \int_{\phi}^{\phi_o} \frac{d\phi}{1+\epsilon_r} = R_o - R_m \int_{\phi}^{\phi_o} (1 - \epsilon_r + \epsilon_r^2 - \epsilon_r^3 + \ldots)\, d\phi \tag{5-A}$$

Since $\epsilon_r \ll 1$ and $R_m = w/\phi_o$, eq. (5-A) can be simplified to give

$$r_i = R_o \left[1 - \frac{w}{R_o}\left(1 - \frac{\phi}{\phi_o}\right) + \frac{w}{R_o}\int_{\phi}^{\phi_o} \frac{\epsilon_r\, d\phi}{\phi_o}\right] \tag{6-A}$$

Thus, the tangential strain is

$$\epsilon_\theta = \frac{\frac{w}{R}\left[1 - \frac{\phi}{\phi_o} - \frac{\sin\phi_o}{\phi_o} + \frac{\sin\phi}{\phi_o}\right] - \frac{w}{R_o}\int_{\phi}^{\phi_o} \frac{\epsilon_r\, d\phi}{\phi_o}}{1 - \frac{w}{R_o}\left(1 - \frac{\phi}{\phi_o}\right) + \frac{w}{R_o}\int_{\phi}^{\phi_o} \frac{\epsilon_r\, d\phi}{\phi_o}} \tag{7-A}$$

It will be shown presently that $\sigma_\theta \gg \sigma_r$, which is almost intuitively obvious in any case. Consequently, the radial strain ϵ_r from eq. (3-A) is about equal to $-\mu\sigma_\theta$. Using this approximation and then invoking the assumption that the higher powers of w/R_o can be neglected, eq. (7-A) reduces to

$$\epsilon_\theta \approx \frac{w}{R_o}\left(1 - \frac{\phi}{\phi_o} - \frac{\sin\phi_o}{\phi_o} + \frac{\sin\phi}{\phi_o}\right) \tag{8-A}$$

Equation (8-A) specifies ϵ_θ in terms of known quantities. The approximations involved in deriving eq. (8-A) amount to neglecting the stretching across the baffle width.

The circumferential stress, according to Hooke's law, eq. (3-A), is

$$\sigma_\theta = \mu\sigma_r + E\left(\frac{w}{R_o}\right)\left(1 - \frac{\phi}{\phi_o} - \frac{\sin\phi_o}{\phi_o} + \frac{\sin\phi}{\phi_o}\right) \tag{9-A}$$

Substituting eq. (9-A) into the in-plane force balance, eq. (1-A), and using the transformation $ds = R_m d\phi = w(d\phi/\phi_o)$, the force balance can be written as

$$\frac{d\sigma_r}{d\phi} + \sigma_r\left(\frac{w}{R_o}\right)(1-\mu)\left(\frac{\cos\phi}{\phi_o}\right) = E\left(\frac{w}{R_o}\right)^2\left(\frac{\cos\phi}{\phi_o}\right)\left(1 - \frac{\phi}{\phi_o} - \frac{\sin\phi_o}{\phi_o} + \frac{\sin\phi}{\phi_o}\right) \tag{10-A}$$

where higher powers of w/R_o have been neglected. With the boundary condition that $\sigma_r = 0$ at $\phi = 0$, the solution of eq. (10-A) is

$$\sigma_r = \frac{E}{\phi_o^2}\left(\frac{w}{R_o}\right)^2\left(\phi_o \sin\phi - \sin\phi_o \sin\phi + \frac{1}{2}\sin^2\phi - \cos\phi - \phi\sin\phi + 1\right) \tag{11-A}$$

and higher powers of w/R_o again have been neglected. This equation can be put in a simpler form by using the series expansions for $\sin\phi$ and $\cos\phi$:

$$\sigma_r = \frac{1}{6}E\phi_o^2\left(\frac{w}{R_o}\right)^2\left(1 + \frac{1}{20}\phi_o^2\right)\left(\frac{\phi}{\phi_o} - \frac{1}{6}\frac{\phi^3}{\phi_o^3}\right) \tag{12-A}$$

This expression is an accurate representation of the way σ_r varies with ϕ whenever $\phi_o \leqslant \pi/4$.

The tangential stresses can be computed from eqs. (9-A) and (12-A):

$$\sigma_\theta = \frac{1}{6}E\phi_o^2\left(\frac{w}{R_o}\right)^2\left(1 + \frac{1}{20}\phi_o^2\right)\left(\frac{\phi}{\phi_o} - \frac{1}{6}\frac{\phi^3}{\phi_o^3}\right) + \frac{1}{6}E\phi_o^2\left(\frac{w}{R_o}\right)\left(1 - \frac{\phi^3}{\phi_o^3}\right) \tag{13-A}$$

A comparison of eq. (13-A) and eq. (12-A) shows that σ_θ is about a factor R_o/w greater than σ_r, which verifies the assumption made earlier about the magnitude of σ_r.

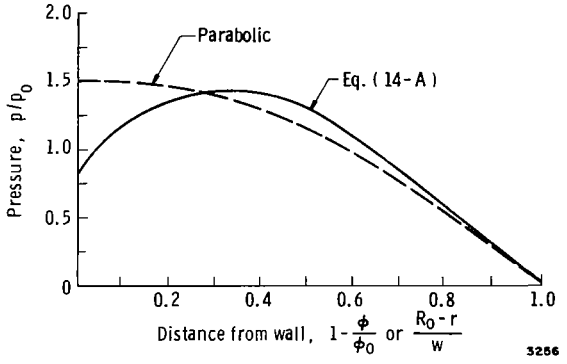

FIGURE 3-A. PREDICTED PRESSURE DISTRIBUTION COMPARED TO ACTUAL PARABOLIC PRESSURE DISTRIBUTION

The pressure loading that causes the baffle to deflect into the assumed circular arc can be computed from the force-balance equation in the normal direction, eq. (2-A). In this equation, the meridional radius of curvature R_m, is w/ϕ_o and the tangential radius of curvature R_θ is $r/\sin\phi$. Neglecting higher powers of w/R_o, the pressure is

$$p = \frac{Et\phi_o^3}{6R_o}\left(\frac{w}{R_o}\right)\left[\left(1 + \frac{1}{20}\phi_o^2\right)\left(\frac{\phi^3}{\phi_o^3} - \frac{1}{6}\frac{\phi^3}{\phi_o^3}\right) + \frac{\phi}{\phi_o} - \frac{1}{6}\phi_o^2\left(\frac{\phi^3}{\phi_o^3}\right)\right] \tag{14-A}$$

(Even though $\sigma_\theta \gg \sigma_r$, both σ_θ and σ_r support the pressure about equally, because $R_m \ll R_\theta$). The pressure given by eq. (14-A) and shown in Figure 3-A is slightly too small near the supported edge of the baffle, compared to the actual parabolic distribution. Nonetheless, the pressure distribution is reasonably close to parabolic over most of the baffle width. The average pressure, according to eq. (14-A), is

$$\bar{p}_o = \frac{1}{\phi_o}\int_0^{\phi_o} p\,d\phi = \frac{Et\phi_o^3}{R_o}\left(\frac{w}{R_o}\right)[0.068\,(1 + 0.05\phi_o^2) + 0.050(1 - 0.023\phi_o^2)] \tag{15-A}$$

For values of ϕ_o less than $\pi/4$, eq. (15-B) is well approximated by

$$\bar{p}_o = 0.118\left(\frac{w}{R_o}\right)\frac{Et\phi_o^3}{R_o} \tag{16-A}$$

which allows the angle ϕ_o (and the meridional and tangential radii of curvatures) to be easily computed when the true average pressure $p_o = \bar{p}_o$ is specified from eq. (4-A).

The maximum stress is the σ_θ stress at $\phi = 0$; the maximum σ_r stress is much less than this. By substituting ϕ_o, as computed from eq. (16-A), for a given p_o, into eq. (13-A), the maximum stress in the baffle is found to be

$$\sigma_{max} = \sigma_\theta(\phi = 0) = 0.69E\left(\frac{w}{R_o}\right)^{1/3}\left(\frac{p_o R_o}{Et}\right)^{2/3} \tag{17-A}$$

Comparison with exact theory.—Equation (17-A) was used to compute σ_{max} for a number of sample cases, and the results were compared to the "exact" finite-element solution mentioned previously. The comparison is shown in Table 1-A. The average pressure p_o for these comparisons was computed from eq. (4-A), by assuming various values of w/R_o, ζ_o/R_o, and d_s/R_o, with ρ, g, and R_o given the realistic values shown in the table. As can be seen, the difference between the two maximum stress predictions is very small regardless of whether the baffle is lightly loaded (small p_o and small w/R_o) or heavily loaded (large p_o and large w/R_o). It can be concluded, then, that the approximate solution gives accurate results over the complete range of the variables, namely: $0.05 \leqslant w/R_o \leqslant 0.15$, $0 \leqslant \zeta_o/R_o \leqslant 0.15$, and $0 \leqslant d_s/R_o \leqslant 0.40$.

TABLE 1-A. COMPARISON OF MAXIMUM STRESS PREDICTED BY APPROXIMATE THEORY AND "EXACT" FINITE-ELEMENT COMPUTER PROGRAM

$\rho = 1.14 \times 10^3$ kg/m^3 $\quad g = 2g_o = 19.6$ m/sec^2 $\quad R_o = 2.54$ m

$E \times 10^{-5}$ newton/m^2	d_s/R_o	w/R_o	ζ/R_o	$p_o/\rho g R_o$	$(t/R_o) \times 10^4$	σ_{max}, newton/m^2 Eq. (17-A)	σ_{max}, newton/m^2 "Exact"
8.3 (Plastic A)	0.15	0.05	0.15	0.0510	0.70	6.20×10^7	5.98×10^7
5.5 (Plastic B)	0.15	0.15	0.15	0.0865	3.50	3.80×10^7	3.78×10^7
77.5 (Aluminum)	0.15	0.10	0.15	0.0713	2.72	8.30×10^7	8.13×10^7
77.5 (Aluminum)	0.05	0.05	0.05	0.0126	0.34	8.30×10^7	8.06×10^7

NOTE: 0.69×10^4 newton/m^2 = 1 lb/in^2.

Incidentally, the baffle thickness t for these calculations was picked so that σ_{max} was a realistic maximum stress for the material; thus, these thicknesses, which range from about 8.6×10^{-5} m (0.0034 in.) to 8.9×10^{-4} m (0.035 in.) are representative of full-scale baffle thickness for a tank of about 500 cm (200 in.) diameter.

Baffle thickness.—The allowable σ_{max} should be less than σ_{yield}, say $\sigma_{max} = \sigma_{yield}/K$ where $K > 1$ is a factor of safety. Thus, eq. (17-A) can also be used to calculate the required minimum baffle thickness for given baffle width, slosh pressure, and material properties:

$$t_{minimum} = 0.57R_o\left(\frac{w}{R_o}\right)^{1/2}\left(\frac{K^{3/2}E^{1/2}p_o}{\sigma_{yield}^{3/2}}\right) \tag{18-A}$$

Thermal stresses.—For this approximate theory, the thermal stresses induced in the baffle when its temperature is lowered can be computed independently of the stresses induced by the slosh pressures. The thermal stresses also satisfy eq. (1-A) (and here $\phi \equiv 0$, that is, the baffle is flat), so they can be included directly in eq. (2-A) along with the pressure-induced stresses to compute a new pressure distribution and average pressure $\bar{p}_o$ to compare with the known p_o.

The thermal stresses are

$$\sigma_\theta = \frac{1}{2}E\bar{\alpha}\Delta T\left[1 + \frac{(R_o - w)^2}{r^2}\right]$$
$$\sigma_r = \frac{1}{2}E\bar{\alpha}\Delta T\left[1 - \frac{(R_o - w)^2}{r^2}\right] \tag{19-A}$$

where $\bar{\alpha}$ is an effective thermal expansion coefficient, including the thermal expansion coefficient and flexibility of the baffle supports. The maximum value of $\bar{\alpha}$ occurs when the supports are perfectly rigid, so that $\bar{\alpha} = \alpha_B - \alpha_T$, which is the difference between the thermal expansion coefficients of the baffle material and the tank walls. The maximum values are $\bar{\alpha}\Delta T \approx 0.005$ to 0.01 for a representative plastic film baffle, aluminum tank walls, and a temperature drop of 200°C (room temperature to LOX boiling temperature), and the thermal stresses are about $0.005\,E$ to $0.01\,E$. For most plastic films, the thermal stresses therefore are about one-third to one-half of the yield stress. Thus, if $K = 3$ in eq. (18-A), the baffle should not be overstressed even if the thermal stresses are neglected. Of course, if complete information about the baffle supporting structure is available, the flexibility of the supports can be evaluated and the thermal stresses can be computed exactly. It is believed, however, that eq. (18-A) with $K = 3$ is sufficiently conservative for design purposes, especially since this formula neglects the contribution of the thermal stresses in supporting the pressure load.

REFERENCES

1. Miles, J. W.: Ring Damping of Free Surface Oscillations in a Circular Tank. *Trans. ASME, Jour. Appl. Mech.*, vol 25, no. 2, June 1958, pp 274-276.

2. Anon: Slosh Suppression. NASA SP-8031, 1969.

3. Silveira, M. A.; Stephens, D. G.; and Leonard, H. W.: An Experimental Investigation of the Damping of Liquid Oscillations in Cylindrical Tanks with Various Baffles. NASA TN D-715, 1961.

4. Summer, I. E.: Experimental Investigation of Slosh-Suppression Effectiveness of Annular-Ring Baffles in Spherical Tanks. NASA TN D-2519, 1964.

5. Schwind, R.; Scotti, R.; and Skogh, J.: Analysis of Flexible Baffles for Damping Tank Sloshing. *Jour. Spacecraft Rockets,* vol 4, no. 1, January 1967, pp 47-53.

6. Stephens, D. G.: Flexible Baffles for Slosh Damping. *Jour. Spacecraft Rockets,* vol. 3, no. 5, May 1966, pp 765-766.

7. Garza, L.R.; and Dodge, F. T.: A Comparison of Flexible and Rigid Baffles for Slosh Suppression. *Jour. Spacecraft Rockets,* vol. 4, no. 6, June 1967, pp. 805-806.

8. Stephens, D. G.; and Scholl, H. F.: Effectiveness of Flexible and Rigid Ring Baffles for Damping Liquid Oscillations in Large-Scale Cylindrical Tanks. NASA TN D-3878, 1967.

9. Kinney, G. F.: **Engineering Properties and Applications of Plastics.** John Wiley and Sons, Inc., 1957.

10. Anon. Cryogenic Materials Data Handbook. Technical Documentary Report, No. ML-TDR-64-280, Air Force Materials Laboratory, August 1964.

11. Landrock, A. H.: Properties of Plastics and Related Materials at Cryogenic Temperatures. Plastec Report No. 20, Picatinny Arsenal, July 1965.

12. Weatherford, W. D., Jr.: LOX-Container-Rupture Fire Hazards. Final Report, Contract NAS 9-7510, Southwest Research Institute, San Antonio, Texas, Oct. 1967.

13. Hoggatt, J. T.: Polymeric Positive Expulsion Bladders for Liquid Oxygen Systems. NASA CR-72418, June 1968.

14. Anon: Propellant Slosh Loads. NASA SP-8009, August 1968.

15. Langner, C. G.: A Preliminary Analysis for Optimum Design of Ring and Partition Antislosh Baffles. Tech. Report No. 7, Contract NAS 8-1555, Southwest Research Institute, San Antonio, Texas, April 1963.

16. Roark, R. J.: **Formulas for Stress and Strain.** Fourth ed., McGraw-Hill Book Co., Inc., 1965.

17. Abramson, H. N., ed: The Dynamic Behavior of Liquids in Moving Containers. NASA SP-106, 1966.

18. Den Hartog, J. P.: **Advanced Strength of Materials.** McGraw-Hill Book Co., Inc., 1952.